Exotic collider signals from the complete phase diagram of minimal universal extra dimensions

Jose A. R. Cembranos, Jonathan L. Feng, and Louis E. Strigari
Department of Physics and Astronomy, University of California, Irvine, California 92697, USA
(Received 21 December 2006; published 8 February 2007)

Minimal universal extra dimensions (mUED) is often thought to predict that the lightest Kaluza-Klein particle (LKP) is the Kaluza-Klein gauge boson B^1, leading to conventional missing energy signals at colliders and weakly interacting massive particle (WIMP) dark matter. In fact, the implications of mUED are far richer: the B^1, charged Higgs boson $H^{\pm 1}$, and graviton G^1 are all possible LKPs, leading to many different phases with distinct signatures. Considering the complete phase diagram, we find predictions for charged or neutral particles with decay lengths of microns to tens of meters; WIMP, superWIMP, or charged relic particles; metastable particles with lifetimes of the order of or in excess of the age of the Universe; and scenarios combining two or more of these phenomena. In the cosmologically preferred region, the Higgs boson mass is between 180 and 245 GeV, the LKP mass is between 810 and 1400 GeV, and the maximal splitting between first Kaluza-Klein modes is less than 320 GeV. This region predicts a variety of exotic collider signals, such as slow charged particles, displaced vertices, tracks with non-vanishing impact parameters, track kinks, and even vanishing charged tracks, all of which provide early discovery possibilities at the Large Hadron Collider.

DOI: 10.1103/PhysRevD.75.036004 PACS numbers: 11.10.Kk, 12.60.−i, 95.35.+d, 98.80.Cq

I. INTRODUCTION

The idea that there may be extra spatial dimensions is an old one, going back at least as far as the work of Kaluza and Klein in the 1920's [1]. Their original idea was untenable, but it has many modern descendants, of which the closest living relative is universal extra dimensions (UED) [2]. In UED, all particles propagate in flat, compact extra dimensions of size 10^{-18} m or smaller. Each known particle has an associated set of heavy partner particles, providing a wealth of possible implications for particle physics and cosmology.

In this study we consider minimal UED (mUED) in which there is one extra dimension of size R compactified on an S^1/Z_2 orbifold, where Z_2 is the action $y \to -y$, with y the coordinate of the extra dimension. Every state of the standard model has a partner particle at Kaluza-Klein (KK) level n with mass nR^{-1}, supplemented by tree-level contributions from electroweak symmetry breaking and radiative corrections [3,4]. In general UED theories, there may also be contributions to the KK masses from mass terms localized on the orbifold boundaries. These contributions would generically violate bounds on flavor and CP violation. To remain consistent with the experiment, a simple assumption, which defines mUED, is that these boundary contributions are absent. The resulting model preserves a discrete parity known as KK-parity, which implies that the lightest KK particle (LKP) is stable and a possible dark matter candidate [5–9].

Minimal UED is therefore an extremely simple, viable extra-dimensional extension of the standard model. It is completely determined by only 2 parameters: m_h, the mass of the standard model Higgs boson, and one new parameter, R, the compactification radius. (In detail, there is also a third parameter, the cutoff scale Λ, but the dependence on Λ is logarithmic and weak, as discussed below.) Precision electroweak measurements require $R^{-1} \gtrsim 250$ GeV [2,10], with other low energy constraints similar or weaker [11,12]. Particle physics alone does not place an upper bound on R^{-1}, but the thermal relic density of LKPs grows with R^{-1}, and LKPs would overclose the Universe for $R^{-1} > 1.5$ TeV [5,13–17], providing strong motivation for considering weak-scale KK particles. For the Higgs boson mass, the direct constraints on the standard model also apply to UED and require $m_h > 114.4$ GeV at 95% confidence limits (CL) [18]. In contrast, however, the indirect bounds on m_h are significantly weakened relative to the standard model, requiring only $m_h < 900$ GeV for $R^{-1} = 250$ GeV and $m_h < 300$ GeV for $R^{-1} = 1$ TeV at 90% CL [10].

Early studies of UED focused on the line in model parameter space defined by $m_h = 120$ GeV [4] and neglected the existence of the KK graviton G^1 [5,6]. Given these assumptions, for $R^{-1} \gtrsim 250$ GeV, the LKP is the hypercharge gauge boson B^1, and these studies therefore focused on missing energy signals at colliders and weakly interacting massive particle (WIMP) dark matter for cosmology. These predictions are similar to those from supersymmetry with R-parity conservation. UED with KK-parity and supersymmetry with R-parity predict different collider event rates for similar spectra, and the different spins of partner particles may be distinguished through, for example, indirect dark matter detection in positrons [6]. Nevertheless, the difficulty of distinguishing UED and supersymmetry has attracted much attention and been a fertile testing ground for future experiments, especially the Large Hadron Collider (LHC) [19].

In fact, however, more recent studies have shown that framework of UED is far richer than indicated above. First,

it was noted that the KK graviton G^1 necessarily exists in any UED model and may be the LKP, leading not to WIMP dark matter, but to superWIMP dark matter, with a completely different set of cosmological and astroparticle signatures [7–9]. Second, studies have now emphasized that, by relaxing the constraint $m_h = 120$ GeV and considering higher values, KK Higgs bosons may become lighter than the B^1. That both of these possibilities may be realized in a general UED model is, perhaps, not surprising. Remarkably, however, all of these complexities arise even in the extremely constrained framework of mUED. Any one of the G^1, B^1, and the charged Higgs boson $H^{\pm 1}$ may be the LKP, leading to many different ''phases'' of parameter space with qualitatively distinct signatures. The ''triple point,'' where $m_{G^1} = m_{B^1} = m_{H^{\pm 1}}$, lies in the heart of parameter space at $(R^{-1}, m_h) \approx (810\ \text{GeV}, 245\ \text{GeV})$, leading to many interesting features.

With this as motivation, we consider here the full parameter space of mUED and its implications for particle physics and cosmology. In Sec. II we present the complete phase diagram of mUED. For reasons given below, we begin by excluding the graviton G^1 from consideration and define phases to be regions with distinct standard model (NLKP, LKP) pairs. With this classification, we explore the collider physics of mUED in Sec. III, and find that long-lived particles with macroscopic decay lengths at colliders are common in the full parameter space.

In Sec. IV, we then include the graviton G^1, and examine each phase in light of cosmological constraints on charged dark matter, diffuse photon spectra, and dark matter thermal relic densities. We find that each phase of parameter space is cosmologically viable, given, for example, a low enough reheat temperature $T_{\text{RH}} > 1$ MeV, justifying the effort made in Sec. III to elucidate the collider implications of every phase. At the same time, for standard cosmological scenarios with $T_{\text{RH}} \gtrsim 10$ GeV, we find that the viable region of parameter space has $180\ \text{GeV} \lesssim m_h \lesssim 245\ \text{GeV}$, $810\ \text{GeV} \lesssim R^{-1} \lesssim 1400\ \text{GeV}$, and a maximal splitting between the LKP and the heaviest $n = 1$ KK state (the KK gluon g^1) is always less than 320 GeV. In addition, this cosmologically favored region of the phase diagram predicts charged particle decays, such as $H^{+1} \to B^1 u\bar{d}$, $B^1 c\bar{s}$, $B^1 e^+ \nu_e$, $B^1 \mu^+ \nu_\mu$, $B^1 \tau^+ \nu_\tau$, with macroscopic decay lengths from microns to tens of meters, leading to the possibility of spectacular signals and early discoveries at the LHC. These predictions are rather striking and differentiate mUED from supersymmetry and essentially all other frameworks for new physics proposed to date. These collider signals, as well as other conclusions and future directions, are presented in Sec. V.

Finally, our conventions and notations are collected in the appendix, along with Feynman rules and other technical details helpful for determining decay widths.

II. MASS SPECTRUM AND PHASE DIAGRAM

As we will see below, although mUED is among the simplest extra-dimensional extensions of the standard model, the spectrum of mUED is remarkably intricate. We will find that there are several LKP candidates, and degeneracies $\lesssim 1$ GeV among the lightest KK states are not uncommon.

Rather than deal immediately with the complexity of this complicated spectrum, we begin in this section by ignoring the existence of the KK graviton G^1. This is beneficial for two reasons. First, because the KK graviton has only cosmological significance, neglecting it allows us to defer cosmological considerations and the accompanying dependence on early universe assumptions to focus on collider physics predictions, which are much more robust. Second, this simplification allows us to divide the parameter space into a manageable number of phases with qualitatively distinct signatures at colliders.

The definition of ''phase'' is, of course, somewhat arbitrary. The simplest option is to divide the parameter space into regions with different LKPs, as a pair of LKPs is produced in every KK event, and so the nature of the LKP determines to a large extent the collider signatures. At the other extreme, one might argue that, viewed in sufficient detail, collider signals depend on the entire KK spectrum, making each point in parameter space a different phase and eliminating the utility of the concept of phases in model parameter space.

For mUED, however, we find that a useful definition of phases lies between these two extremes. As we will see, in mUED, the nature of both the LKP and the next-to-lightest KK particle (NLKP) are important, as they both impact *qualitatively* what signatures are predicted. In this section, we therefore, exclude the G^1 from consideration and divide the parameter space into phases with distinct standard model (NLKP, LKP) pairs. In mUED, and without taking into account the KK graviton, the following KK particles may be either the LKP or the NLKP: the hypercharge gauge boson B^1, the 3 SU(2) singlet leptons e_R^1, μ_R^1, and τ_R^1, the charged Higgs boson $H^{\pm 1}$, and the CP-odd Higgs boson A^1. The complete spectrum for mUED, including one-loop corrections, was first presented in Ref. [3]. Here we reproduce the formulae that determine the masses of these states.

The mUED spectrum is completely determined by 3 parameters,

$$R^{-1}, \quad m_h, \quad \Lambda, \tag{1}$$

where R is the compactification radius, m_h is the Higgs boson mass, and Λ is the cutoff scale. As seen below, masses depend only logarithmically on Λ. The dependence is therefore weak, and we have checked that, for the range $10 \leq \Lambda R \leq 50$, our main results are essentially independent of Λ. For numerical results, we take $\Lambda R = 20$ throughout this study.

The G^1, $H^{\pm 1}$, and A^1 masses are

$$m_{G^1} = R^{-1}, \tag{2}$$

$$m^2_{H^{\pm 1}} = R^{-2} + m^2_W + \delta m^2_H, \tag{3}$$

$$m^2_{A^1} = R^{-2} + m^2_Z + \delta m^2_H, \tag{4}$$

where the radiative correction to the Higgs boson masses is

$$\delta m^2_H = \left(\frac{3}{2}g^2 + \frac{3}{4}g'^2 - \frac{m^2_h}{v^2}\right)\frac{\ln(\Lambda^2 R^2)}{16\pi^2}R^{-2}, \tag{5}$$

and $v \simeq 246$ GeV is the Higgs boson vacuum expectation value. Note that the electroweak symmetry breaking and radiative corrections to m_{G^1} are negligible, and the corrections to $m_{H^{\pm 1}}$ and m_{A^1} are not only small, but may also be either positive or negative, depending on m_h.

The KK charged lepton mass matrix, where l_L and l_R denote SU(2) doublet and singlet states, respectively, is

$$\begin{pmatrix} R^{-1} + \delta m_{l^1_L} & m_l \\ m_l & -R^{-1} - \delta m_{l^1_R} \end{pmatrix}, \tag{6}$$

where

$$\delta m_{l^1_L} = \left(\frac{27}{16}g^2 + \frac{9}{16}g'^2\right)\frac{\ln(\Lambda^2 R^2)}{16\pi^2}R^{-1}, \tag{7}$$

$$\delta m_{l^1_R} = \frac{9}{4}g'^2\frac{\ln(\Lambda^2 R^2)}{16\pi^2}R^{-1}. \tag{8}$$

For the viable regions of parameter space, the lighter eigenstate is very nearly a pure l^1_R state, and so we refer to it as l^1_R. We diagonalize the mass matrix of Eq. (6) (and also the matrix of Eq. (9) below) in obtaining numerical results, but the l^1_R mass is very well approximated by the lower right-hand entry of the mass matrix. The KK leptons e^1_R, μ^1_R, τ^1_R are extremely degenerate, with $m_{\tau^1_R(\mu^1_R)} - m_{e^1_R} \approx m^2_{\tau(\mu)}R \sim 1$ MeV(10 keV).

The neutral electroweak gauge boson masses are, in the basis (B^1, W^1),

$$\begin{pmatrix} R^{-2} + \frac{1}{4}g'^2v^2 + \delta m^2_{B^1} & \frac{1}{4}g'gv^2 \\ \frac{1}{4}g'gv^2 & R^{-2} + \frac{1}{4}g^2v^2 + \delta m^2_{W^1} \end{pmatrix}, \tag{9}$$

where

$$\delta m^2_{B^1} = \left(-\frac{39}{2}\frac{g'^2\zeta(3)}{16\pi^4} - \frac{g'^2}{6}\frac{\ln(\Lambda^2 R^2)}{16\pi^2}\right)R^{-2}, \tag{10}$$

$$\delta m^2_{W^1} = \left(-\frac{5}{2}\frac{g^2\zeta(3)}{16\pi^4} + \frac{15g^2}{2}\frac{\ln(\Lambda^2 R^2)}{16\pi^2}\right)R^{-2}, \tag{11}$$

and ζ is the Riemann zeta function, with $\zeta(3) \simeq 1.202$. For the viable regions of parameter space, the lighter eigenstate is approximately a pure B^1 state, and so we refer to it as B^1. Its mass is well approximated by the upper left-hand entry of the mass matrix. Note that the contribution from electroweak symmetry breaking may be canceled by the radiative correction.

For the reasons given above, we now ignore the G^1 and divide the parameter space into regions with distinct (NLKP, LKP) pairs. The result is given in Fig. 1. There are four phases, which, from lower left to upper right, have the (NLKP, LKP) combinations 1: (l^1_R, B^1), 2: $(H^{\pm 1}, B^1)$, 3: $(B^1, H^{\pm 1})$, and 4: $(A^1, H^{\pm 1})$. Note that the line $m_h = 120$ GeV lies completely in Phase 1 (for 115 GeV $\lesssim R^{-1} \lesssim 1430$ GeV), but for larger m_h, the $H^{\pm 1}$ becomes the NLKP. For even larger m_h, the $H^{\pm 1}$ becomes the LKP, and for still larger m_h, the lightest two KK particles are the two Higgs bosons A^1 and $H^{\pm 1}$. Although we are temporarily excluding the KK graviton from consideration here, for later reference, we have also plotted the line on which $m_{G^1} = m_{B^1}$. The "triple point," where $m_{B^1} = m_{G^1} = m_{H^{\pm 1}}$, is at $(R^{-1}, m_h) \approx (810\ \text{GeV}, 245\ \text{GeV})$ for $\Lambda R = 20$, and its location is essentially independent of Λ in the range $10 \leq \Lambda R \leq 50$.

In Fig. 2, we show the mass splittings $\Delta m = m_{\text{NLKP}} - m_{\text{LKP}}$ in the full parameter space. Remarkably, the mass splittings are only of the order of 1 to 10 GeV throughout the full phase diagram. One might expect splittings of the order of $R^{-1}/(16\pi^2)$, $m^2_W R \sim 10$ GeV; modest additional cancellations arising from effects highlighted above in fact make this an overestimate in most of parameter space.

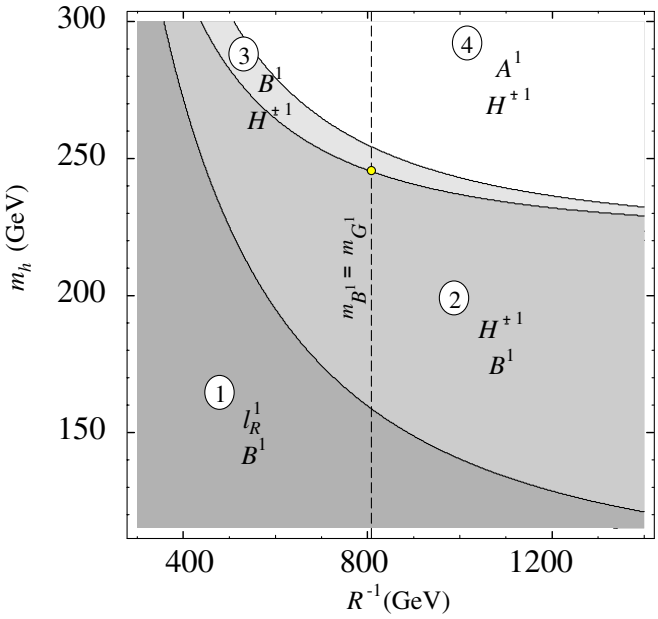

FIG. 1 (color online). The complete collider phase diagram of mUED in the (R^{-1}, m_h) plane, where R is the compactification radius, and m_h is the Higgs boson mass. The KK graviton G^1 has been excluded from consideration, and the standard model (NLKP, LKP) pairs in each phase are as indicated. We have set $\Lambda R = 20$. For reference, the line on which $m_{G^1} = m_{B^1}$ is also plotted. The "triple point," where $m_{B^1} = m_{G^1} = m_{H^{\pm 1}}$, is at $(R^{-1}, m_h) \approx (810\ \text{GeV}, 245\ \text{GeV})$.

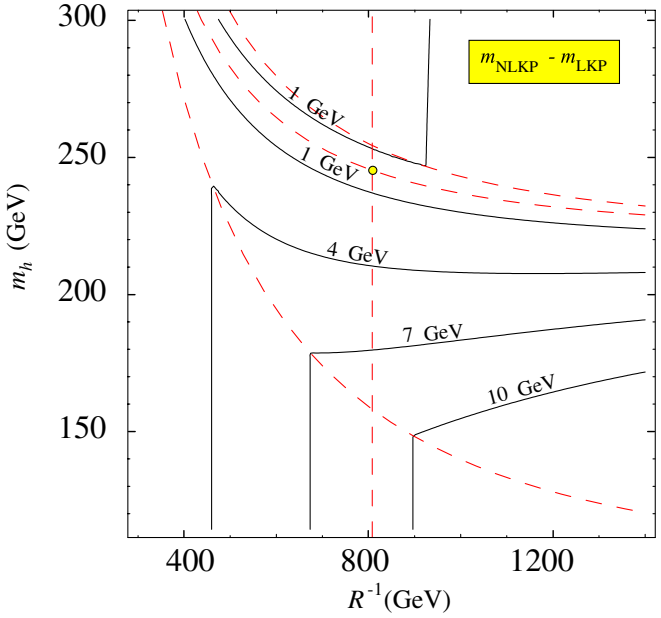

FIG. 2 (color online). Mass splittings (in GeV) between the standard model NLKP and LKP in the full phase diagram of mUED. The dashed lines are the boundaries between different phases shown in Fig. 1. We have set $\Lambda R = 20$.

III. LONG-LIVED PARTICLES AT COLLIDERS

In Sec. II, we found fractional degeneracies of 0.001 to 0.01 throughout the mUED phase diagram. These degeneracies suppress NLKP decay widths, such that NLKPs produced in colliders may decay at points macroscopically separated from the interaction point. In this section we present numerical results for the most relevant decays. Two- and three-body decay widths and lengths are given in Figs. 3 and 4, respectively, and the NLKP decay lengths throughout mUED parameter space are given in Fig. 5. Analytical formulae for the decay widths, along with useful results for calculating them, are given in the appendix.

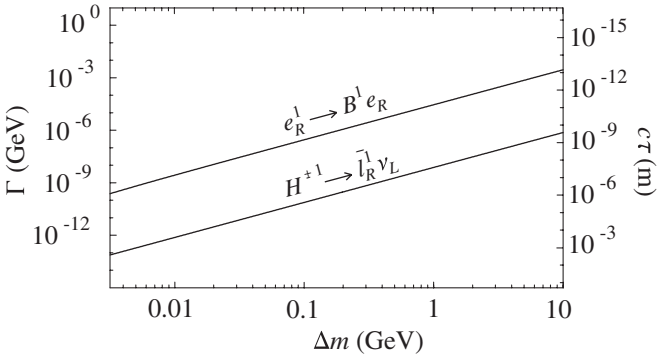

FIG. 3. Decay widths and decay lengths as a function of the mass splitting Δm between KK states for the two-body decays indicated. We have fixed the decaying particle's mass to $M = 1$ TeV.

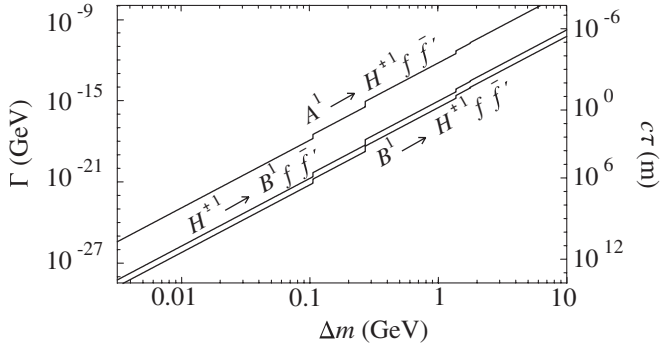

FIG. 4. Decay widths and decay lengths as a function of the mass splitting Δm between KK states for the three-body decays indicated. We have fixed the decaying particle's mass to $M = 1$ TeV. The discontinuities result from setting $m_f = m_{\tilde{f}'} = 0$ for all kinematically accessible final states. We include the ud final state above the $\pi\pi$ threshold.

In Phase 1, the NLKP to LKP decay is $l_R^1 \to B^1 l_R$, which is a two-body decay suppressed only by the mass degeneracy discussed above. As can be seen in Eq. (A17) and Fig. 3, for mass splittings 100 MeV $\lesssim \Delta m \lesssim$ 10 GeV the decay lengths are 10^{-9} m $\gtrsim c\tau \gtrsim 10^{-13}$ m (for $R^{-1} = 1$ TeV). To observe displaced vertices or nonvanishing impact parameters at colliders, decay lengths should be greater than about 10 μm. The $l_R^1 \to B^1 l_R$ decay lengths are, then, too short to be observable in any part of Phase 1.

Are there other particles in Phase 1 that can have macroscopic decay lengths? Although the answer is no, this question merits discussion. The 4 lightest standard model

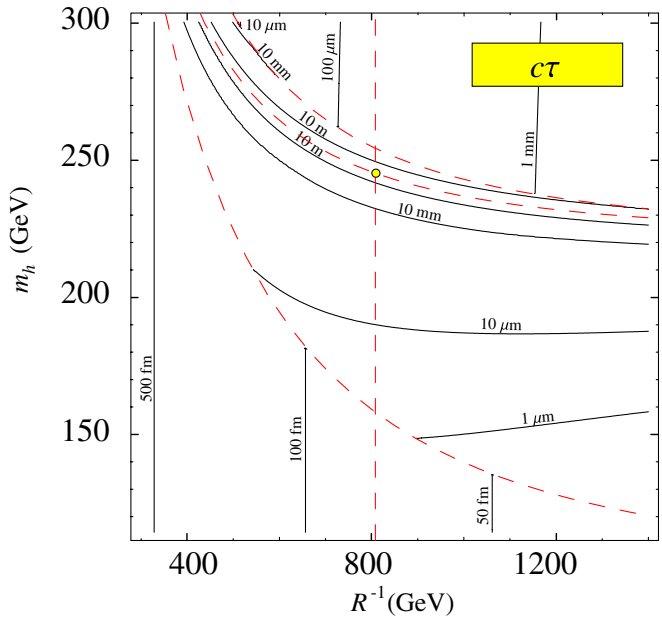

FIG. 5 (color online). Standard model NLKP decay lengths in the full phase space of mUED. We have set $\Lambda R = 20$ and neglected the KK graviton G^1. The dashed curves are the boundaries of phases shown in Fig. 1.

states in most of Phase 1 are, in decreasing order of mass, $(A^1, H^{\pm 1}, l_R^1, B^1)$. The charged Higgs boson decays through $H^{\pm 1} \to B^1 f \bar{f}'$ and $H^{+1} \to \bar{l}_R^1 \nu_l$. The former is three-body and parametrically suppressed by $(\Delta m)^5/(m_W^2 M^2)$. As can be seen in Eq. (A28) and Fig. 4, this by itself would lead to a macroscopic decay length. The latter decay is two-body, but suppressed by Yukawa couplings. Unfortunately, this suppression for the τ decay mode is insufficient to keep the decay length macroscopic. Of course, there is an extremely thin region in Phase 1 along the border between Phase 1 and 2 in which $H^{+1} \to \bar{\mu}_R^1 \nu_\mu$ is kinematically allowed but $H^{+1} \to \bar{\tau}_R^1 \nu_\tau$ is not, which would make the $H^{\pm 1}$ decay length observably long, but we do not consider this further.

In Phase 1 the A^1 may decay through $A^1 \to H^{\pm 1} f \bar{f}'$, $B^1 \gamma$, $\bar{l}_R^1 l_R$. (Note that $A^1 \to B^1 Z^* \to B^1 f \bar{f}$ is not allowed, because the tree-level AZZ coupling is forbidden by CP-invariance, and, of course, the tree-level $AZ\gamma$ coupling is absent because the A is neutral.) The first two are highly suppressed; $A^1 \to H^{\pm 1} f \bar{f}'$ is parametrically suppressed by $(\Delta m)^5/m_W^4$, a huge suppression given the degeneracies of mUED, and $A^1 \to B^1 \gamma$ is a two-body decay, but is loop-suppressed. However, $\Gamma(A^1 \to \bar{l}_R^1 l_R) = \Gamma(H^{\pm 1} \to \bar{l}_R^1 \nu_l)$, and so, once again, the Yukawa coupling decay is not sufficiently suppressed to produce a long-lived track.

We conclude, then, that there are no long-lived tracks in Phase 1. It is rather remarkable, however, that the NNLKP and the NNNLKP can be so close to being long-lived, despite the many decay channels open to them.

In Phase 2 the NLKP to LKP decay, $H^{\pm 1} \to B^1 f \bar{f}'$, is three-body. The parametric phase space suppression of $(\Delta m)^5/(m_W^2 M^2)$ leads to decay lengths of 20 cm for $\Delta m = 1$ GeV, as seen in Eq. (A28) and Fig. 4. As a result, displaced vertices and nonzero impact parameters are expected for much of Phase 2 from the decays $H^{+1} \to B^1 e_R^+ \nu_e$, $B^1 \mu_R^+ \nu_\mu$, $B^1 \tau_R^+ \nu_\tau$, $B^1 u \bar{d}$, $B^1 c \bar{s}$. The standard model fermions produced are extremely soft, creating a difficult challenge for collider experiments. We discuss these issues in Sec. V.

Approaching the upper boundary of Phase 2, the H^{+1} and B^1 may be arbitrarily degenerate. For $\Delta m \lesssim 0.4$ GeV, the H^{+1} is essentially stable for collider phenomenology (again, see Eq. (A28) and Fig. 4), resulting in signals associated with slow, metastable charged particles, such as highly ionizing tracks and time-of-flight signals.

In Phase 3, the B^1 and $H^{\pm 1}$ exchange roles relative to Phase 2, and the NLKP decay is $B^1 \to H^{\pm 1} f \bar{f}'$. For small mass splittings $\Delta m \ll M$, this decay width differs from that for $H^{\pm 1} \to B^1 f \bar{f}'$ only by the average over 3 initial spin polarizations, and so the decay length is 3 times longer, as shown in Eq. (A32) and Fig. 4. This decay length is longer than 10 mm for most of Phase 3, and so the B^1 is potentially observable as a long-lived particle. Note, however, that in contrast to Phase 2, the parent particle here is neutral and the heavy daughter particle is charged.

As one approaches the Phase 3/Phase 2 boundary in Phase 3, of course, the splitting between the B^1 and H^{+1} may be arbitrarily small. For $\Delta m \lesssim 0.5$ GeV, the B^1 lifetime is so large that one expects the standard missing energy signal.

Finally, in Phase 4 the NLKP decay is $A^1 \to H^{\pm 1} f \bar{f}'$; the decay length is given in Eq. (A36) and Fig. 4. The A^1 and $H^{\pm 1}$ masses are similarly controlled by R^{-1} and m_h, and so their mass splitting is almost constant throughout the phase diagram. In Phase 4, $\Delta m = m_{A^1} - m_{H^{\pm 1}}$ varies from 0.7 GeV to 1.8 GeV, and the A^1 decay length varies from 10 μm to 1 mm. This prediction is quite robust, and the decay length is therefore likely in the observable range.

IV. COSMOLOGICAL CONSTRAINTS

So far we have neglected the KK graviton G^1 and ignored cosmological constraints. In this section, we reintroduce G^1 and discuss the three most stringent cosmological bounds on mUED: null searches for exotic charged stable particles, the diffuse photon spectrum, and the thermal relic density of WIMP dark matter.

Throughout this section, we assume that G^1 production during reheating after inflation is negligible. This may very well *not* be the case, as G^1 production is extremely effective in UED [9], and may be significant even for reheating temperatures $T_{\rm RH} \sim$ TeV. The possibility of KK graviton production during reheating has been examined in Refs. [9,20].

With this assumption, the KK graviton is cosmologically relevant when it is the LKP. In Fig. 6, we present the

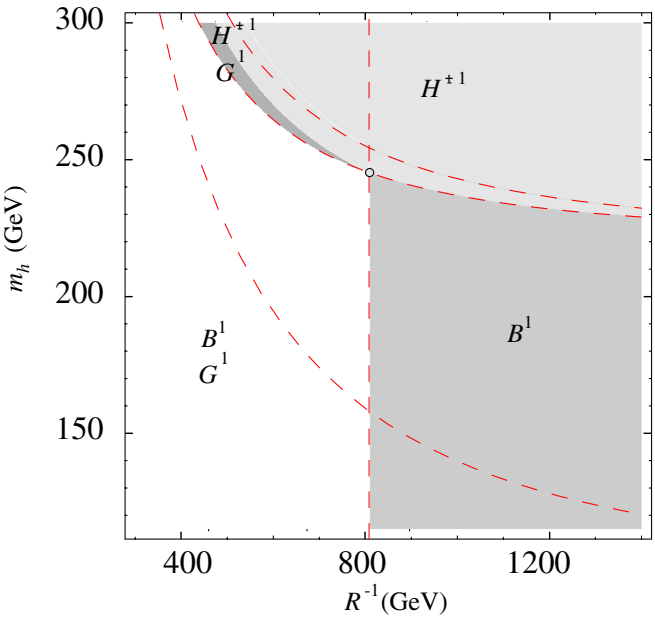

FIG. 6 (color online). The complete cosmological phase diagram of mUED in the (R^{-1}, m_h) plane. Phases are determined by the LKP when it is a standard model KK particle (H^{+1} or B^1), and by the (NLKP, LKP) combination when the LKP is the KK graviton G^1. The dashed lines denote boundaries of the collider phase diagram, as given in Fig. 1. We have set $\Lambda R = 20$.

complete cosmological phase diagram of mUED, where phases are defined by the LKP when it is a standard model KK particle, and by the (NLKP, LKP) combination when the LKP is the KK graviton G^1.

A. Charged stable particles

In Phases 3 and 4, the lightest standard model KK particle is the charged Higgs boson $H^{\pm 1}$. Including the KK graviton G^1, we find that the $H^{\pm 1}$ is not the lightest KK particle everywhere in this region: in a thin region along the lower left border of Phase 3, G^1 is lighter than $H^{\pm 1}$ by a GeV or less (for $R^{-1} \gtrsim 300$ GeV). The lifetime for $H^{\pm 1} \to G^1 f \bar{f}'$ is given in Eq. (A56); parametrically, it depends on $(\Delta m)^7/(m_W^2 M_4^2 m_{H^{\pm 1}}^2)$, where $M_4 \simeq 1.72 \times 10^{18}$ GeV is the 4-dimensional Planck mass. It is therefore extraordinarily suppressed and typically many orders of magnitude greater than the age of the Universe. Effectively, then, the $H^{\pm 1}$ is stable throughout Phases 3 and 4. (It is interesting to note, however, that this feature can easily change if the mUED is minimally extended to include KK right-handed neutrinos [21]. In these scenarios, the KK right-handed neutrinos effectively act as new superWIMPs, and can ameliorate cosmological and astrophysical constraints.)

The possibility of a stable charged particle is often considered to be completely excluded by bounds on charged dark matter. On the other hand, it is also true that such particles can be diluted away to insignificant abundances by a period of inflation. The tension between these two statements may be put on a quantitative footing by asking the question in the following way: Assume inflation diluted the $H^{\pm 1}$ density to zero. The Universe then reheats, however, and Higgs bosons $H^{\pm 1}$ are regenerated. What is the maximal reheating temperature $T_{\rm RH}$ such that the resulting $H^{\pm 1}$ density is consistent with bounds on charged relic particles? The lower the maximal $T_{\rm RH}$ is, the more cosmologically disfavored the scenario. If the maximal $T_{\rm RH}$ is less than 1 MeV, the required reheat temperature is inconsistent with big bang nucleosynthesis and the scenario may be considered excluded by cosmology.

Bounds on $T_{\rm RH}$ were considered in exactly this context in Ref. [22]. For stable charged particles X with masses 100 GeV $\lesssim m_X \lesssim 1$ TeV, this study found that the extremely stringent bound $n_X/n_H \lesssim 10^{-28}$ [23] on the number density of charge $+1$ X particles relative to that of hydrogen atoms in sea water requires $T_{\rm RH} \lesssim 1$ MeV, effectively excluding such particles. However, for 1 TeV $\lesssim m_X \lesssim 1.6$ TeV, the experimental limit weakens drastically to $n_X/n_H \lesssim 4 \times 10^{-17}$ [24], and $T_{\rm RH}$ as high as $\sim$1 GeV is possible. Although $T_{\rm RH} \sim$ GeV is still extremely low from a model building point of view, we know little about the Universe at temperatures above 1 MeV, and such a possibility cannot be excluded.

We conclude that Phases 3 and 4 with $R^{-1} \lesssim 1$ TeV is excluded cosmologically, but the rest of Phases 3 and 4 is allowed, provided the reheating temperature after inflation satisfies $T_{\rm RH} \lesssim$ GeV. Of course, in all cases, the $H^{\pm 1}$ relic density is insufficient to be a significant amount of dark matter.

B. Diffuse photon flux

In Phases 1 and 2 with $R^{-1} < 810$ GeV, the KK graviton G^1 is lighter than the lightest standard model KK particle, the B^1. The decay $B^1 \to G^1 \gamma$ is gravitational and the $B^1 - G^1$ mass splitting is typically a few GeV or less. The resulting decays, given in Eq. (A51), are therefore extremely suppressed. For G^1 masses greater than 300 GeV, the maximum mass splitting between the G^1 and B^1 is about 1.5 GeV. Equation (A51) then implies that the B^1 will decay after matter-radiation equality, and these decays are thus strongly constrained by cosmological observations.

For injected energies $\sim$GeV in the redshift range of interest ($z \sim 10^3 - 0$), the decay photons redshift, but the flux of photons is otherwise unattenuated by scattering processes with the intergalactic medium or cosmic microwave background photons [25]. The fact that the $B^1 \to G^1 \gamma$ decays fall in this transparency window is quite unique. If the decay photons were injected with energies greater than 10 to 1000 GeV, depending on the decay redshift, a large optical depth would result from pair-production off of cosmic microwave background photons. For lower injected energies below 10 keV, decay photons would lose energy from scattering off of free electrons and atoms. From Eq. (A51), a B^1 decaying today will produce photons with injected energy $\sim$20 MeV.

Constraints on late decaying B^1 particles have been considered in the context of the superWIMP dark matter scenario in Ref. [9]. The diffuse photon spectrum from $B^1 \to G^1 \gamma$ decays is [9]

$$\frac{d\phi}{dE} = \frac{3}{8\pi} \frac{N_{\rm in}}{V_0 E_{\rm in}} \frac{t_0}{\tau} \left[\frac{E}{E_{\rm in}}\right]^{1/2} e^{-(E/E_{\rm in})^{3/2}(t_0/\tau)} \Theta(E_{\rm in} - E), \tag{12}$$

where $N_{\rm in}$ is the number of B^1 particles at freezeout, V_0 and t_0 are the present volume and age of the Universe, respectively, and τ is the B^1 lifetime. $E_{\rm in} = (m_{B^1}^2 - m_{G^1}^2)/2m_{B^1}$ is the initial energy of the produced photons, which is related to the present energy through $E_{\rm in} = (1 + z_{\rm in})E$, where $z_{\rm in}$ is the redshift when produced. For $\Delta m = m_{B^1} - m_{G^1} \ll m_{B^1}$, $\tau \propto (\Delta m)^{-3}$, and $E_{\rm in} \approx \Delta m$, and both are independent of the overall KK mass scale.

We compare this diffuse photon spectrum to the diffuse background spectrum in the MeV regime from COMPTEL [26],

$$\frac{d\phi}{dE} \simeq 1.1 \times 10^{-4} \left[\frac{E}{5\ {\rm MeV}}\right]^{-2.4} {\rm MeV}^{-1}\,{\rm cm}^{-2}\,{\rm s}^{-1}\,{\rm sr}^{-1}, \tag{13}$$

valid over an energy range $E \sim 0.8$–30 MeV. To apply the

constraints from the observations, we demand that the integrated flux from B^1 decays be less than the integrated flux from the observed background over the energy range of interest. In principle, this bound could be made more strict by comparing the spectrum of photons from decays to the power-law spectrum in Eq. (13). However, since the photon background excludes such a large class of models, we find the integrated flux bound an accurate criterion for our purposes.

For a given number density $N_{\rm in}$ the diffuse photon flux excludes certain lifetimes τ. These constraints are given in Fig. 7, where we express the value of $N_{\rm in}$ in terms of Ω_{B^1} normalized to $\Omega_{\rm DM}$ for $m_{B^1} = 800$ GeV. All parameters above the curve are excluded by our criterion.

In the relevant region of the mUED phase diagram (Phase 1 and 2 with $R^{-1} < 810$ GeV), $\tau \gtrsim 10^{12}$ sec. Assuming reheating temperatures $T_{\rm RH} \gtrsim m_{B^1}/25$, the B^1's are produced with significant thermal relic densities, and these models violate the bounds of Fig. 7. This region of the phase diagram is therefore also excluded given standard cosmological assumptions. However, as in Sec. IV A, for lower reheat temperatures, bounds from the diffuse photon flux may be evaded.

Our bound assumes that the B^1 decays during matter domination, and we have neglected the impact of the clustering around dark matter halos. Figure 7 shows that the larger the B^1 lifetime τ the more stringent the constraint on Ω_{B^1}. Of course, for extremely long lifetimes τ greater than the age of the Universe, the constraint weakens again. For $\tau \gtrsim t_0$, it is possible to derive a strict bound from diffuse particles in the galactic halo, which would also contribute to the diffuse gamma ray background [27].

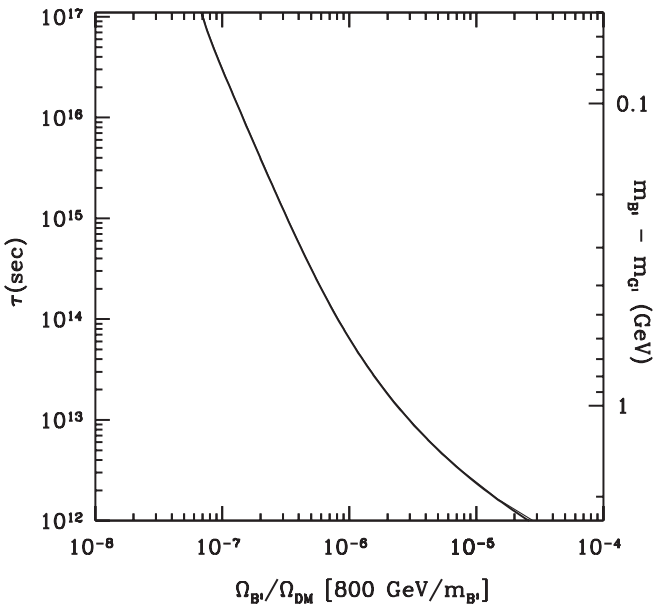

FIG. 7. Constraints on the B^1 relic density (if they had not decayed) from requiring that the integrated flux of photons from $B^1 \to G^1\gamma$ not exceed the observed MeV diffuse photon flux. The region above the curve is excluded.

C. WIMP thermal relic density

In Phases 1 and 2 with $R^{-1} > 810$ GeV, the B^1 is lighter than the G^1, and so it is absolutely stable and a WIMP dark matter candidate. Given standard cosmological assumptions, the B^1 thermal relic may then be determined. The first calculation of Ref. [5] has now been refined by the inclusion of the full mUED spectrum, radiative corrections to KK particle masses, $n = 2$ resonances, and all coannihilation processes [13–17].

The results of Ref. [17] are reproduced in Fig. 8, which is discussed more fully in Sec. V. Requiring that the B^1 thermal relic density not exceed the observed dark matter density provides yet another cosmological constraint on the mUED phase diagram, excluding the lower right-hand portion of the (R^{-1}, m_h) plane.

Of course, as with the other cosmological constraints, the WIMP relic density constraint may also be avoided by assuming a lower reheating temperature, which, in this case, is somewhat below $m_{B^1}/25$.

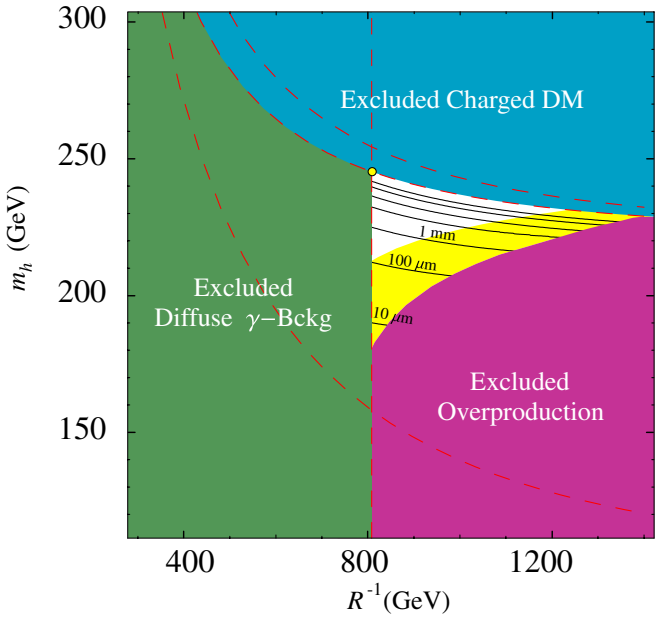

FIG. 8 (color online). The cosmologically preferred region of the complete phase diagram of mUED. The G^1 has been included, and the dark shaded regions are excluded by the cosmological constraints on stable charged relics, the diffuse photon flux, and WIMP overproduction, as indicated. In the preferred region, the light shaded region is from Ref. [17] and shows where the B^1 thermal relic density is within 2σ of the Wilkinson Microwave Anisotropy Probe (WMAP) central value for nonbaryonic dark matter. Contours of constant decay length $c\tau =$ 10 μm, 100 μm, 1 mm, ..., 1 m, 10 m are also plotted (only the lowest few are labeled).

V. SUMMARY AND LHC SIGNALS

In this study we have analyzed the complete parameter space of mUED, in many senses the simplest extra-dimensional extension of the standard model. In mUED all particles propagate in one additional flat, compact dimension, and the model introduces only one additional free parameter, the compactification radius R of the extra dimension. Despite this extremely simple structure, we find that mUED encompasses a wide variety of seemingly exotic and spectacular predictions for particle colliders and cosmology, once the entire parameter space is considered.

Our results are summarized in Figs. 1, 5, and 8. We began by setting aside the KK graviton G^1 and cosmological considerations, leading to the complete collider phase diagram of Fig. 1. We find that mUED supports four distinct standard model (NLKP, LKP) combinations, or phases, with qualitatively different implications for signatures. Potentially most spectacular is the prediction of long-lived particles at colliders. The NLKP decay lengths throughout parameter space are given in Fig. 5. Long-lived TeV-scale particles might appear exotic and unlikely. However, the example of mUED provides a simple, concrete counterexample that highlights a generic possibility: in any theory where TeV-scale particles receive identical tree-level mass contributions M from some new source, the typical splittings one might expect from radiative or electroweak symmetry breaking effects are of the order of $M/(16\pi^2)$, $m_W^2/M \sim 10$ GeV. Modest additional cancellations can bring this down to $\sim$1 GeV, and such splittings lead to macroscopic decay lengths in three-body decays.

In mUED, the KK spectrum is highly degenerate, and so strongly interacting KK particles will be produced with large rates at the LHC. Long-lived NLKP tracks will therefore presumably be most easily identified in the cascades decays of KK quarks and gluons. Such events will be characterized by many jets and missing transverse energy, which will satisfy trigger criteria, and the jets will fix the interaction point. The possible signals are:

(i) Phase 1: Prompt decays $l_R^1 \to B^1 l_R$, where $l = e$, μ, τ, the mass splitting between KK states is $\Delta m \sim \mathcal{O}$ (GeV), and the final state lepton is consequently very soft.

(ii) Phase 2: Decays $H^{\pm 1} \to B^1 f\bar{f}'$, where $f\bar{f}' = e^+\nu_e$, $\mu^+\nu_\mu$, $u\bar{d}$, $\tau^+\nu_\tau$, $c\bar{s}$, where the decay length is $c\tau \gtrsim 100$ nm (for $R^{-1} \lesssim 1400$ GeV) and may be effectively infinite for collider phenomenology. Again $\Delta m \sim \mathcal{O}$ (GeV), and the final state fermions are very soft. Depending on the observability of the final state fermions, the exotic signatures could include nonprompt decays producing displaced vertices, tracks with nonvanishing impact parameters, track kinks, or even disappearing charged ($H^{\pm 1}$) tracks that mysteriously vanish after passing through only part of the detector. In the parameter region where the $H^{\pm 1}$ is effectively stable, it may be produced at low velocities, resulting in time-of-flight anomalies and highly ionizing tracks.

(iii) Phase 3: Decays $B^1 \to H^{\pm 1} f\bar{f}'$, where the $f\bar{f}'$ pairs are as in Phase 2, with decay length typically satisfying $c\tau \gtrsim 10$ mm (except in a tiny region, in which could be even shorter than 10 μm), and again $\Delta m \sim \mathcal{O}$ (GeV), and the final state standard model fermions are very soft. The possible signatures are as above, with the exception that, since the NLKP is neutral and the LKP is charged in this case, NLKP events could instead be seen as charged ($H^{\pm 1}$) tracks that mysteriously *appear* somewhere in the detector.

(iv) Phase 4: Decays $A^1 \to H^{\pm 1} f\bar{f}$, where $f = e$, μ, τ, u, d, s, c, and the decay length is constrained to the relatively narrow range 10 μm $\lesssim c\tau \lesssim 1$ mm. The signatures are as in Phase 3.

Following these collider results, we reintroduced the KK graviton G^1 and considered cosmological constraints. For a low enough reheating temperature after inflation, (portions of) all four phases, even Phases 3 and 4 with charged LKPs, were viable, justifying our efforts to classify their collider signatures.

At the same time, much of the phase diagram is excluded if one assumes a standard cosmology with reheat temperature above $R^{-1}/25$. The final results are given in Fig. 8. Phases 3 and 4 are excluded by bounds on stable charged particles, Phases 1 and 2 with $R^{-1} < 810$ GeV are excluded by bounds from the observed diffuse MeV photon flux, and Phases 1 and 2 with high R^{-1} are excluded because WIMPs are overproduced through thermal freezeout.

The resulting cosmologically preferred region is bounded on all sides, resulting in the ''triangle'' shown in Fig. 8. In this region

(i) The Higgs boson mass lies in the range 180 GeV $\lesssim m_h \lesssim$ 245 GeV. This region is allowed by indirect bounds on m_h, and implies the ''golden'' four lepton signatures for Higgs bosons at the LHC.

(ii) The compactification radius satisfies 810 GeV $\lesssim R^{-1} \lesssim$ 1400 GeV. The LKP mass is therefore in this range, and the splitting between the LKP and the heaviest $n = 1$ KK particle, the KK gluon g^1, is never more than 320 GeV. KK particles will therefore be copiously produced at the LHC. On the contrary, none of these new particles would be produced directly at the International Linear Collider operating at center-of-mass energies below 1.5 TeV.

(iii) The NLKP to LKP decay is $H^{\pm 1} \to B^1 f\bar{f}'$, with decay lengths satisfying $c\tau \gtrsim 4$ μm, with effectively no upper bound. Generically, then, long-lived tracks are predicted for the LHC, leading to the wealth of novel signatures detailed above.

These features differentiate mUED from essentially all other proposals for new electroweak physics. In particular, they differ markedly from supersymmetry, in which all of

these features would be viewed as extraordinarily unnatural.

We have not examined the cross sections for, and backgrounds to, NLKP production at the LHC in these various phases. Such an analysis is, of course, required if one is to conclude anything about the observability of these interesting phenomena. We have also not considered the extension of mUED to include neutrino masses and KK right-handed neutrinos [21]. The existence of these new states at mass R^{-1} provides an alternative nongravitational decay to the decays to G^1 discussed here. Given the simplicity of mUED and the results obtained here, all of these directions merit further investigation.

We note also that the mUED scenario provides a simple particle physics framework for seemingly exotic cosmology. For example, it is remarkable that the values of R^{-1} that give significant B^1 thermal relic densities also give extremely degenerate B^1 and G^1 states. Throughout the mUED parameter space, it is quite easy to envision scenarios in which the dark matter is produced from the decays of cold, thermal relics with a wide variety of lifetimes. For example, we can consider decays at $\sim 10^6$ s, as in the superWIMP framework, or during the matter-dominated epoch of the Universe, as in metaCDM [28], or even lifetimes longer than the age of the Universe. In the context of cosmological small-scale structure, dark matter from decays may help alleviate problems facing standard cold dark matter (CDM) models [28–31]. These unique phenomenological signatures suggest new avenues for investigating the identity of dark matter.

ACKNOWLEDGMENTS

We thank H.-C. Cheng, K. Matchev, A. Rajaraman, and F. Takayama for stimulating correspondence and conversations. The work of J. A. R. C. and J. L. F. is supported in part by NSF CAREER Grant No. PHY-0239817, NASA Grant No. NNG05GG44G, and the Alfred P. Sloan Foundation. The work of J. A. R. C. is also supported by the FPA 2005-02327 project (DGICYT, Spain). L. E. S. is supported in part by the Center for Cosmology at UC Irvine.

APPENDIX A: DECAY WIDTH ANALYSIS

1. Notation and approximations

We use the following notation for the electromagnetic fine structure constant, the weak mixing angle, the hypercharge and weak coupling constants, and the 4-dimensional Planck mass:

$$\alpha = \frac{e^2}{4\pi} \simeq \frac{1}{137}, \frac{1}{128}, \tag{A1}$$

$$\sin^2\theta_W \simeq 0.238, 0.231, \tag{A2}$$

$$g' = \frac{e}{\cos\theta_W}, \tag{A3}$$

$$g = \frac{e}{\sin\theta_W}, \tag{A4}$$

$$M_4 = \frac{1}{\sqrt{16\pi G_N}} = \frac{1}{\sqrt{2}} M_* \simeq 1.72 \times 10^{18}\ \text{GeV}. \tag{A5}$$

In the first 2 lines, the first numerical values given are appropriate for processes with momentum transfer of ~ 1 GeV, and the second values are those at the weak scale appropriate for evaluation of the KK mass spectrum.

Throughout this paper, we consider decays $X(M, p) \to Y(m_1, q_1) Z_2(m_2, q_2)[Z_3(m_3, q_3)]$, with mass and momentum labels given, where X and Y are heavy KK level $n = 1$ particles and Z_2 and Z_3 are light KK level $n = 0$ (standard model) particles. We neglect the effects of standard model particle masses in all open decay channels. With this approximation, the two- and three-body decay widths are

$$\Gamma_2 = \frac{1}{16\pi} \frac{M^2 - m_1^2}{M^3} \overline{|\mathcal{M}|^2}, \tag{A6}$$

$$\Gamma_3 = \int_{m_1^2}^{M^2} dm_{12}^2 \int_0^{(M^2 - m_{12}^2)(m_{12}^2 - m_1^2)/m_{12}^2} dm_{23}^2 \frac{1}{256\pi^3 M^3} \overline{|\mathcal{M}|^2}, \tag{A7}$$

respectively, where $m_{ij}^2 \equiv (q_i + q_j)^2$.

In presenting the results for decay widths, it is convenient to define

$$\Delta m \equiv M - m_1, \tag{A8}$$

$$y \equiv \frac{m_1^2}{M^2}, \tag{A9}$$

$$N_C = \sum_i N_C^i, \tag{A10}$$

where N_C is the sum of color factors over all kinematically accessible channels. For three-body decays, we include only diagrams mediated by off-shell standard model gauge bosons, and neglect all others, which are mediated by much heavier KK particles and are suppressed by small Yukawa couplings. For example, for $H^{\pm 1} \to B^1 f \bar{f}'$, we include the contribution from $H^{\pm 1} \to B^1 W^{\pm *} \to B^1 f \bar{f}'$ but neglect the contributions from $H^{\pm 1} \to f \bar{f}'^{1*}$, $\bar{f}' f^{1*} \to B^1 f \bar{f}'$. For all three-body decays, we also assume $\Delta m \ll m_W$.

Finally, in the width formulae below, the symbol $\approx$ appears before expressions that are valid assuming $\Delta m \ll M$.

2. Two-body nongravitational decays

Feynman rules for the relevant vertices are

$$l_R^n B_\mu^m \bar{l}_R^{n-m}: \ -ig' \gamma_\mu, \tag{A11}$$

$$H^{-n}\bar{l}_R^m \nu_l^{n-m}\colon\ -i\frac{g}{\sqrt{2}}\frac{m_l}{m_W}P_L, \tag{A12}$$

$$A^n \bar{l}_R^m l_L^{n-m}\colon\ -i\frac{g}{\sqrt{2}}\frac{m_l}{m_W}\gamma^5 P_L. \tag{A13}$$

The decay widths are

$$\Gamma(l_R^1 \to B^1 l_R) = \frac{g'^2}{16\pi}\frac{M}{y}(1-y)^2(1+2y) \tag{A14}$$

$$\approx \frac{3\alpha}{\cos^2\theta_W}\frac{(\Delta m)^2}{M} \tag{A15}$$

$$\simeq 2.87\times 10^{-5}\ \text{GeV}\left[\frac{\Delta m}{\text{GeV}}\right]^2\left[\frac{\text{TeV}}{M}\right] \tag{A16}$$

$$\simeq \left[6.87\times 10^{-12}\ \text{m}\left[\frac{\text{GeV}}{\Delta m}\right]^2\left[\frac{M}{\text{TeV}}\right]\right]^{-1} \tag{A17}$$

and

$$\Gamma(H^{+1} \to \bar{l}_R^1 \nu_l) = \Gamma(A^1 \to \bar{l}_R^1 l_L) \tag{A18}$$

$$= \frac{g^2}{32\pi}\frac{m_l^2}{m_W^2}M(1-y)^2 \tag{A19}$$

$$\approx \frac{\alpha}{2\sin^2\theta_W}\frac{m_l^2}{m_W^2}\frac{(\Delta m)^2}{M} \tag{A20}$$

$$\simeq 8.10\times 10^{-9}\ \text{GeV}\frac{m_l^2}{m_\tau^2}\left[\frac{\Delta m}{\text{GeV}}\right]^2\left[\frac{\text{TeV}}{M}\right] \tag{A21}$$

$$\simeq \left[2.44\times 10^{-8}\ \text{m}\frac{m_\tau^2}{m_l^2}\left[\frac{\text{GeV}}{\Delta m}\right]^2\left[\frac{M}{\text{TeV}}\right]\right]^{-1}. \tag{A22}$$

3. Three-body nongravitational decays

Feynman rules for the relevant KK vertices are

$$H^{\pm n}B^n W^{\mp}\colon\ i\frac{g'}{2}m_W, \tag{A23}$$

$$A^n(p)H^{\pm n}(q_1)W_\mu^{\mp}\colon\ \frac{g}{2}(p+q_1)_\mu. \tag{A24}$$

The decay widths are

$$\Gamma(H^{\pm 1} \to B^1 f\bar{f}') = \frac{N_C g^2 g'^2}{49152\pi^3}\frac{M^5}{m_W^2 m_1^2} \times[(1-y)(1+y+73y^2+9y^3) + 12y^2(3+4y)\ln y] \tag{A25}$$

$$\approx \frac{N_C\alpha^2}{80\pi\sin^2\theta_W\cos^2\theta_W}\frac{(\Delta m)^5}{m_W^2 M^2} \tag{A26}$$

$$\simeq 1.96\times 10^{-16}\ \text{GeV}N_C\left[\frac{\Delta m}{\text{GeV}}\right]^5\left[\frac{\text{TeV}}{M}\right]^2 \tag{A27}$$

$$\simeq \left[1.01\ \text{m}\frac{1}{N_C}\left[\frac{\text{GeV}}{\Delta m}\right]^5\left[\frac{M}{\text{TeV}}\right]^2\right]^{-1}, \tag{A28}$$

$$\Gamma(B^1 \to H^{\pm 1} f\bar{f}') = \frac{N_C g^2 g'^2}{147456\pi^3}\frac{M^3}{m_W^2} \times[(1-y)(9+73y+y^2+y^3) + 12y^2(4+3y)\ln y] \tag{A29}$$

$$\approx \frac{N_C\alpha^2}{240\pi\sin^2\theta_W\cos^2\theta_W}\frac{(\Delta m)^5}{m_W^2 M^2} \tag{A30}$$

$$\simeq 6.52\times 10^{-17}\ \text{GeV}N_C\left[\frac{\Delta m}{\text{GeV}}\right]^5\left[\frac{\text{TeV}}{M}\right]^2 \tag{A31}$$

$$\simeq \left[3.03\ \text{m}\frac{1}{N_C}\left[\frac{\text{GeV}}{\Delta m}\right]^5\left[\frac{M}{\text{TeV}}\right]^2\right]^{-1}, \tag{A32}$$

and

$$\Gamma(A^1 \to H^{\pm 1} f\bar{f}') = \frac{N_C g^4}{12288\pi^3}\frac{M^5}{m_W^4} \times[(1-y)(1-7y-7y^2+y^3) - 12y^2\ln y] \tag{A33}$$

$$\approx \frac{N_C\alpha^2}{60\pi\sin^4\theta_W}\frac{(\Delta m)^5}{m_W^4} \tag{A34}$$

$$\simeq 1.40\times 10^{-13}\ \text{GeV}N_C\left[\frac{\Delta m}{\text{GeV}}\right]^5 \tag{A35}$$

$$\simeq \left[1.41\ \text{mm}\frac{1}{N_C}\left[\frac{\text{GeV}}{\Delta m}\right]^5\right]^{-1}. \tag{A36}$$

4. Gravitational interactions

Feynman rules for gravitons in UED have been presented in Ref. [9]. Here we abstract those most relevant for the phenomenology of the lightest KK states.

The graviton interactions are given by

$$\mathcal{L}_{\text{int}} = \sum_n \frac{1}{2M_4}G_{\mu\nu}^n T_+^{n\mu\nu}, \tag{A37}$$

where the sum is over KK levels. The stress-energy tensor receives contributions from scalars, fermions, and gauge bosons of the form

$$T^{n\mu\nu}_{+H} = \sum_{m=0}^{n}[(\eta^{\mu\rho}\eta^{\nu\sigma} + \eta^{\mu\sigma}\eta^{\nu\rho} - \eta^{\mu\nu}\eta^{\sigma\rho})D_\rho H^{m\dagger} D_\sigma H^{n-m} + \eta^{\mu\nu} m_H^2 H^{m\dagger} H^{n-m}], \tag{A38}$$

$$T^{n\mu\nu}_{+\psi} = \sum_{m=0}^{n}\Big[\eta^{\mu\nu}(\bar\psi^m_L i\gamma^\rho D_\rho \psi^{n-m}_L - m_{n-m}\bar\psi^m_R\psi^{n-m}_L) - \frac{1}{2}\bar\psi^m_L i\gamma^\mu D^\nu\psi^{n-m}_L - \frac{1}{2}\bar\psi^m_L i\gamma^\nu D^\mu\psi^{n-m}_L - \frac{1}{2}\eta^{\mu\nu}\partial^\rho(\bar\psi^m_L i\gamma_\rho\psi^{n-m}_L) + \frac{1}{2}\eta^{\mu\nu}(m_m + m_{n-m})(\bar\psi^m_R\psi^{n-m}_L) + \frac{1}{4}\partial^\mu(\bar\psi^m_L i\gamma^\nu\psi^{n-m}_L) + \frac{1}{4}\partial^\nu(\bar\psi^m_L i\gamma^\mu\psi^{n-m}_L) + (R\leftrightarrow L)\Big], \tag{A39}$$

$$T^{n\mu\nu}_{+B} = \sum_{m=0}^{n}\Big[F^{m\mu\rho}F^{n-m\nu}_\rho - \frac{1}{4}\eta^{\mu\nu}F^m_{\rho\sigma}F^{n-m\rho\sigma} + m_n m_{n-m}\Big(B^{m\mu}B^{n-m\nu} - \frac{1}{2}\eta^{\mu\nu}B^n_\rho B^{n-m\rho}\Big)\Big], \tag{A40}$$

where $\psi^0_R(x) = 0$, $m_n = n/R$, D is the covariant derivative, and $F^m_{\mu\nu} \equiv \partial_\mu B^m_\nu - \partial_\nu B^m_\mu$.

The sum over graviton polarizations is

$$\sum_i \epsilon^{ni}_{\mu\nu}(k)\epsilon^{ni*}_{\sigma\rho}(k) = 2\Big(\eta_{\mu\rho} - \frac{k_\mu k_\rho}{m_n^2}\Big)\Big(\eta_{\nu\sigma} - \frac{k_\nu k_\sigma}{m_n^2}\Big) + 2\Big(\eta_{\mu\sigma} - \frac{k_\mu k_\sigma}{m_n^2}\Big)\Big(\eta_{\nu\rho} - \frac{k_\nu k_\rho}{m_n^2}\Big) - \frac{4}{3}\Big(\eta_{\mu\nu} - \frac{k_\mu k_\nu}{m_n^2}\Big)\Big(\eta_{\rho\sigma} - \frac{k_\rho k_\sigma}{m_n^2}\Big). \tag{A41}$$

5. Two-body gravitational decays

Feynman rules for the relevant KK vertices are

$$G^n_{\mu\nu}\bar\psi^m(p)\psi^{n-m}(q_2)\colon\ i\frac{1}{4M_4}\Big[\eta_{\mu\nu}[(\gamma^\rho q_{2\rho} - m_{n-m}) - (\gamma^\rho p_\rho - m_m)] - \frac{1}{2}(p+q_2)_\mu\gamma_\nu - \frac{1}{2}(p+q_2)_\nu\gamma_\mu\Big], \tag{A42}$$

$$G^n_{\mu\nu}B^m_\alpha(p)B^{n-m}_\beta(q_2)\colon\ i\frac{1}{2M_4}\Big[\eta_{\alpha\beta}p_\mu q_{2\nu} - \eta_{\mu\alpha}p_\beta q_{2\nu} - \eta_{\nu\beta}p_\mu q_{2\alpha} + \eta_{\mu\alpha}\eta_{\nu\beta}(p\cdot q_2) - \frac{1}{2}\eta_{\mu\nu}(\eta_{\alpha\beta}(p\cdot q_2) - p_\beta q_{2\alpha}) + m_n m_{n-m}\Big(\eta_{\mu\alpha}\eta_{\nu\beta} - \frac{1}{2}\eta_{\mu\nu}\eta_{\alpha\beta}\Big) + (\alpha\leftrightarrow\beta)\Big]. \tag{A43}$$

The decay widths are

$$\Gamma(l^1_R \to G^1 l_R) = \frac{1}{96\pi}\frac{M^7}{M_4^2 m_1^4}(1-y)^4(2+3y) \tag{A44}$$

$$\approx \frac{5}{6\pi}\frac{(\Delta m)^4}{M_4^2 M} \tag{A45}$$

$$\simeq 8.97\times10^{-41}\ \mathrm{GeV}\Big[\frac{\Delta m}{\mathrm{GeV}}\Big]^4\Big[\frac{\mathrm{TeV}}{M}\Big] \tag{A46}$$

$$\simeq \Big[7.34\times10^{15}\ \mathrm{s}\Big[\frac{\mathrm{GeV}}{\Delta m}\Big]^4\Big[\frac{M}{\mathrm{TeV}}\Big]\Big]^{-1} \tag{A47}$$

and

$$\Gamma(B^1 \to G^1\gamma) = \frac{\cos^2\theta_W}{144\pi}\frac{M^7}{M_4^2 m_1^4}(1-y)^3(1+3y+6y^2) \tag{A48}$$

$$\approx \frac{5\cos^2\theta_W}{9\pi}\frac{(\Delta m)^3}{M_4^2} \tag{A49}$$

$$\simeq 4.55\times10^{-38}\ \mathrm{GeV}\Big[\frac{\Delta m}{\mathrm{GeV}}\Big]^3 \tag{A50}$$

$$\simeq \Big[1.45\times10^{13}\ \mathrm{s}\Big[\frac{\mathrm{GeV}}{\Delta m}\Big]^3\Big]^{-1}. \tag{A51}$$

6. Three-body gravitational decays

The relevant KK interaction vertex is

$$H^{\pm n}(p)G^n_{\mu\nu}W^\mp_\rho\colon\ i\frac{m_W}{2M_4}(\eta_{\mu\rho}\eta_{\nu\sigma} + \eta_{\mu\sigma}\eta_{\nu\rho} - \eta_{\mu\nu}\eta_{\rho\sigma})p^\sigma. \tag{A52}$$

The decay width is

$$\Gamma(H^{\pm1}\to G^1 f\bar f') = \frac{N_C g^2}{13824\pi^3}\frac{M^9}{m_W^2 M_4^2 m_1^4}[(1-y)(1-5y-5y^2 - 245y^3 - 50y^4 + 4y^5) - 60y^3(2+3y)\ln y] \tag{A53}$$

$$\approx \frac{N_C 2\alpha}{63\pi^2\sin^2\theta_W}\frac{(\Delta m)^7}{m_W^2 M_4^2 M^2} \tag{A54}$$

$$\simeq 5.58 \times 10^{-51}\ \mathrm{GeV} N_C \left[\frac{\Delta m}{\mathrm{GeV}}\right]^7 \left[\frac{\mathrm{TeV}}{M}\right]^2 \qquad \text{(A55)}$$

$$\simeq \left[1.18 \times 10^{26}\ \mathrm{s}\, \frac{1}{N_C}\left[\frac{\mathrm{GeV}}{\Delta m}\right]^7 \left[\frac{M}{\mathrm{TeV}}\right]^2\right]^{-1}. \qquad \text{(A56)}$$

[1] T. Kaluza, Sitzungsber. Preuss. Akad. Wiss. Berlin (Math. Phys.) **K1**, 966 (1921); O. Klein, Z. Phys. **37**, 895 (1926); Surv. High Energy Phys. **5**, 241 (1986).

[2] T. Appelquist, H.-C. Cheng, and B. A. Dobrescu, Phys. Rev. D **64**, 035002 (2001).

[3] H. C. Cheng, K. T. Matchev, and M. Schmaltz, Phys. Rev. D **66**, 036005 (2002).

[4] H. C. Cheng, K. T. Matchev, and M. Schmaltz, Phys. Rev. D **66**, 056006 (2002).

[5] G. Servant and T. M. Tait, Nucl. Phys. **B650**, 391 (2003).

[6] H. C. Cheng, J. L. Feng, and K. T. Matchev, Phys. Rev. Lett. **89**, 211301 (2002).

[7] J. L. Feng, A. Rajaraman, and F. Takayama, Phys. Rev. Lett. **91**, 011302 (2003).

[8] J. L. Feng, A. Rajaraman, and F. Takayama, Phys. Rev. D **68**, 063504 (2003).

[9] J. L. Feng, A. Rajaraman, and F. Takayama, Phys. Rev. D **68**, 085018 (2003).

[10] T. Appelquist and H. U. Yee, Phys. Rev. D **67**, 055002 (2003); T. Flacke, D. Hooper, and J. March-Russell, Phys. Rev. D **73**, 095002 (2006); **74**, 019902(E) (2006); I. Gogoladze and C. Macesanu, Phys. Rev. D **74**, 093012 (2006).

[11] K. Agashe, N. G. Deshpande, and G. H. Wu, Phys. Lett. B **514**, 309 (2001).

[12] T. Appelquist and B. A. Dobrescu, Phys. Lett. B **516**, 85 (2001).

[13] M. Kakizaki, S. Matsumoto, Y. Sato, and M. Senami, Phys. Rev. D **71**, 123522 (2005).

[14] M. Kakizaki, S. Matsumoto, Y. Sato, and M. Senami, Nucl. Phys. **B735**, 84 (2006).

[15] F. Burnell and G. D. Kribs, Phys. Rev. D **73**, 015001 (2006).

[16] K. Kong and K. T. Matchev, J. High Energy Phys. 01 (2006) 038.

[17] M. Kakizaki, S. Matsumoto, and M. Senami, Phys. Rev. D **74**, 023504 (2006).

[18] R. Barate *et al.* (LEP Working Group for Higgs Boson Searches), Phys. Lett. B **565**, 61 (2003).

[19] For a review, see C. Macesanu, Int. J. Mod. Phys. A **21**, 2259 (2006).

[20] N. R. Shah and C. E. M. Wagner, Phys. Rev. D **74**, 104008 (2006).

[21] S. Matsumoto, J. Sato, M. Senami, and M. Yamanaka, hep-ph/0607331.

[22] A. Kudo and M. Yamaguchi, Phys. Lett. B **516**, 151 (2001); see also G. F. Giudice, E. W. Kolb, and A. Riotto, Phys. Rev. D **64**, 023508 (2001).

[23] P. F. Smith, J. R. J. Bennett, G. J. Homer, J. D. Lewin, H. E. Walford, and W. A. Smith, Nucl. Phys. **B206**, 333 (1982).

[24] T. Yamagata, Y. Takamori, and H. Utsunomiya, Phys. Rev. D **47**, 1231 (1993).

[25] X. L. Chen and M. Kamionkowski, Phys. Rev. D **70**, 043502 (2004).

[26] P. Sreekumar, F. W. Stecker, and S. C. Kappadath, AIP Conf. Proc. No. 510 (AIP, New York, 2004), p. 459.

[27] J. A. R. Cembranos, J. L. Feng, and L. Strigari (unpublished).

[28] L. E. Strigari, M. Kaplinghat, and J. S. Bullock, astro-ph/0606281.

[29] K. Sigurdson and M. Kamionkowski, Phys. Rev. Lett. **92**, 171302 (2004).

[30] M. Kaplinghat, Phys. Rev. D **72**, 063510 (2005).

[31] J. A. R. Cembranos, J. L. Feng, A. Rajaraman, and F. Takayama, Phys. Rev. Lett. **95**, 181301 (2005).